Electronic Supplementary Material (ESI) for Materials Horizons.

Supporting information

Intelligent matter endows reconfigurable temperature and humidity sensations for in-sensor computing

Tao Guo[1], Jiawei Ge[1,2], Yixuan Jiao[1], Youchao Teng[1], Bai Sun[3], Wen Huang[4,5], Hatameh Asgarimoghaddam[1], Kevin P. Musselman[1], Yin Fang[6], Y. Norman Zhou[1*], and Yimin A. Wu[1*]

[1]Department of Mechanical and Mechatronics Engineering, and Waterloo Institute of Nanotechnology, University of Waterloo, Waterloo, Ontario N2L 3G1, Canada

[2]College of Materials Science and Technology, Jiangsu Key Laboratory of Materials and Technology for Energy Conversion, Nanjing University of Aeronautics and Astronautics, Nanjing, 210016, China

[3]Frontier Institute of Science and Technology (FIST), Xi'an Jiaotong University, No.28, Xianning West Road, Xi'an, Shaanxi 710049, P.R. China

[4]New Energy Technology Engineering Laboratory of Jiangsu Province, School of Science, Nanjing University of Posts and Telecommunications, Nanjing 210023, China

[5]State Key Laboratory of Silicon Materials, Zhejiang University, Hangzhou 310027, China

[6] School of Chemical and Biomedical engineering, Nanyang Technological University, Singapore

* Corresponding authors.

E-mail: yimin.wu@uwaterloo.ca (Y. A. Wu), nzhou@uwaterloo.ca (Y. N. Zhou).

Keywords: Intelligent matter, memristor, temperature and humidity, reconfigurable sensation, in-sensor computing

Experimental section

1.1 Device fabrication:

The Ag/CIGSe/Mo and Mo/CIGSe/Mo devices were fabricated by magnetron sputtering and electrochemical deposition. The Mo/CIGSe/Mo device was used as a comparative trial to investigate resistive switching mechanisms. The Mo layer was deposited by direct current sputtering as the bottom electrode. A shadow mask was used to obtain a patterned Mo electrode. The width of the strip was approximately 100 μm. Then, the CIGSe active layer was formed via the electrodeposition process. To prepare the reaction bath, 2.5 mM $CuCl_2 \cdot 2H_2O$, 2.4 mM $InCl_3$, 6 mM $GaCl_3$, 240 mM LiCl, 4.5 mM H_2SeO_3 were dissolved in DI water. All chemicals used in this experiment were purchased from Sigma-Aldrich. Besides, pHydrion (pH 3.00) was employed as the buffer. HCl drops were added to adjust the electrolyte pH to 2 - 3. The electrodeposition process was carried out with an electrochemical workstation (CHI Model 660E Series Electrochemical Analyzer/Workstation). A conventional 3-electrode setup was used. The CIGSe film was obtained by applying a constant potential (-0.63 V in this work) to the working electrode. Relative smooth and density CIGSe can be obtained on the patterned Mo electrode. Then, the Ag (or Mo) strip electrode was deposited on the top of the CIGSe to form a capacitor-like sandwich structure.

1.2 Materials and device characterization:

The optical micrograph of the device was taken by an optical microscope (Oxford BX51M). The surface morphology of the CIGSe film and cross-section of the device was characterized by SEM (UltraPlus FESEMs). The composition information was measured by EDS (UltraPlus FESEMs). The grazing incidence X-ray diffraction (GIXRD) was carried out to characterize the crystalline structure of CIGSe (PANalytical X'Pert PRO system, $Cu_{K\alpha}$ irradiation, $\lambda =$

1.5406 Å). The Raman spectrum was measured by the Renishaw micro-Raman spectrometer (laser wavelength of 633nm, red He-Ne). The surface valence states were tested by X-ray photoelectron spectroscopy (XPS, Thermo-VG Scientific ESCALab 250). The electrical measurement of the fabricated devices was performed on a Keithley 2985A source meter.

1.3 Theoretical material simulation:

Density functional theory calculations were performed on the platform of CP2K software. The Gaussian Plane method was based on double-ζ MOLOPT basis sets (DZVP-MOLOPT-SR-GTH) and Goedecker-Teter-Hutter (GTH) pseudopotentials. The convergence criterion was 1×10^{-6} and the cut-off energy was set as 450 Ry. Periodic models with vacuum space were chosen to describe the interaction between CIGSe and Ag clusters. Firstly, the creation of the CIGSe model with vacuum space was optimized. And then, the Ag cluster was adsorbed on the CIGSe model for ab intio molecular dynamics calculations (AIMD) in the ensemble-canonical ensemble (NVT). The time step was set as 1 fs for 2000 steps under the temperature of 303K. Similarly, the O- functional group generated due to the existence of H_2O molecules was used to bound on the surface of CIGSe model (labeled as CIGSe-O), and further were applied by AIMD calculations under the same parameters. Metadynamics calculations of free energy were carried out to investigate the reaction mechanism, the temperature was set at 303 K. Based on two collective variables (CV): the distance of Ag atom on XZ plane (CV1) and YZ plane (CV2). These simulations allow Ag atom to relax in Z direction with the minimum activation free energy.

Supplementary Figures:

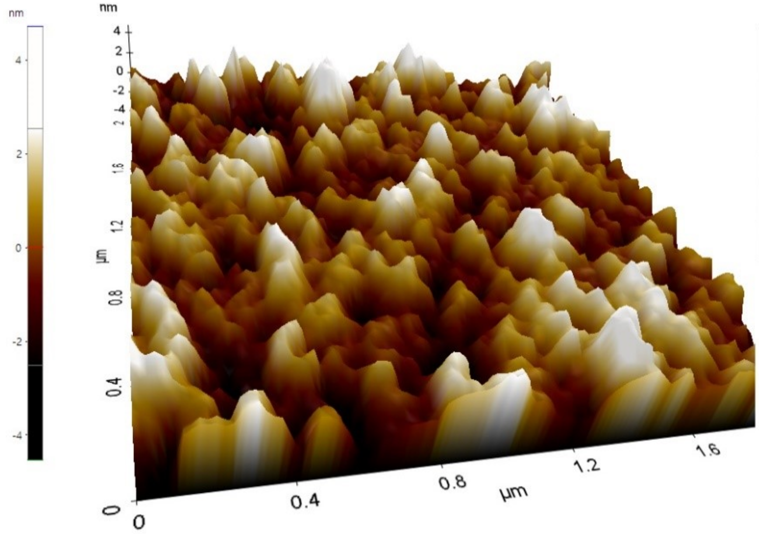

Fig. S1. Atomic force microscope (AFM) image of the CIGSe film.

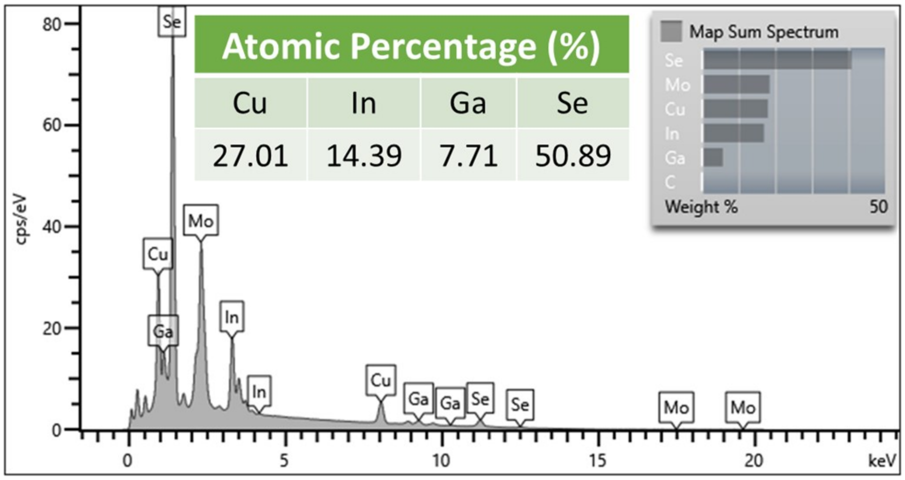

Atomic Percentage (%)

Cu	In	Ga	Se
27.01	14.39	7.71	50.89

Fig. S2. Energy-dispersive X-ray (EDX) spectrum of the CIGSe film. The insert table summarizes the atomic percentage of four elements.

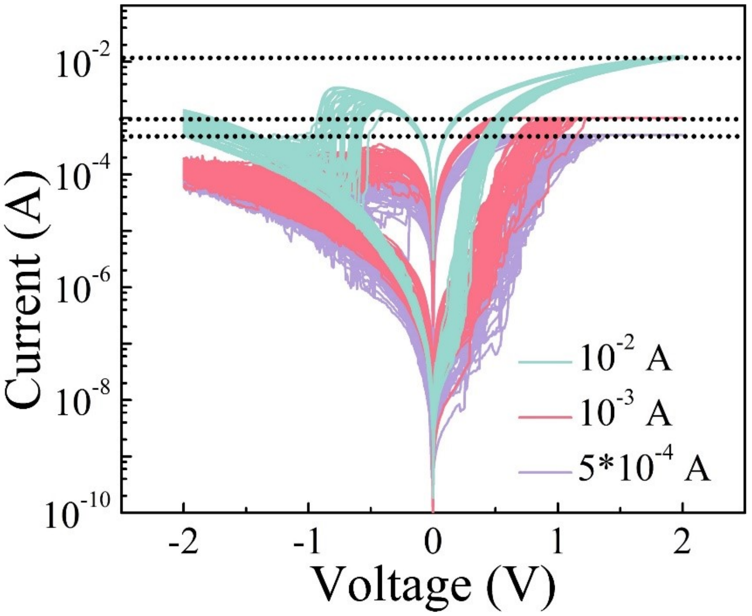

Fig. S3. DC switching cycle test under different compliance currents (CCs). 100 switching cycles for each test.

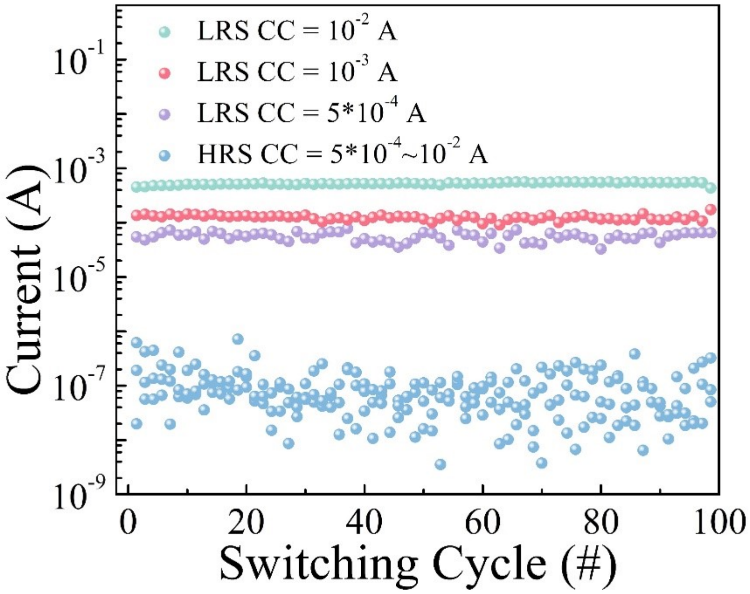

Fig. S4. Resistance states distribution under different compliance currents (CCs).

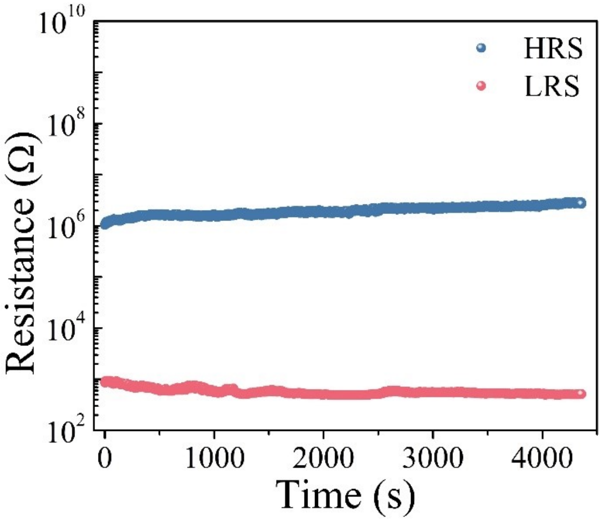

Fig. S5. The retention time of the HRS and LRS.

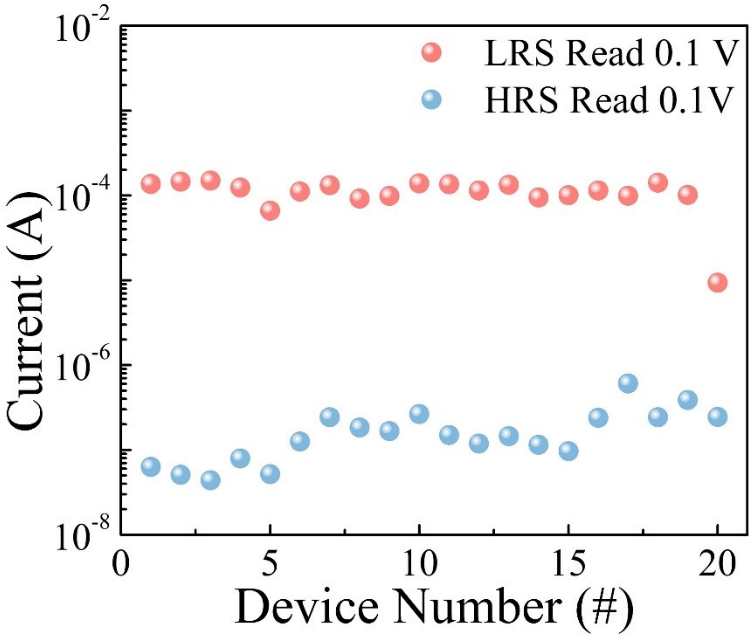

Fig. S6. The device-to-device variation. The results are from the direct current (DC) switching cycle test. The read voltage was 0.1 V for both HRS and LRS.

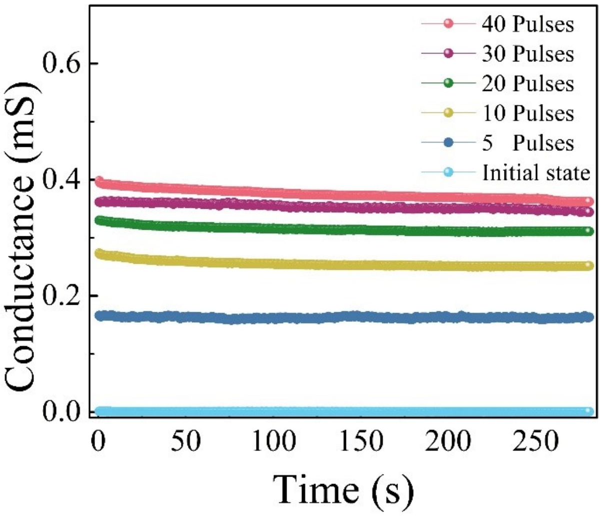

Fig. S7. Retention time of different states under different pulse numbers.

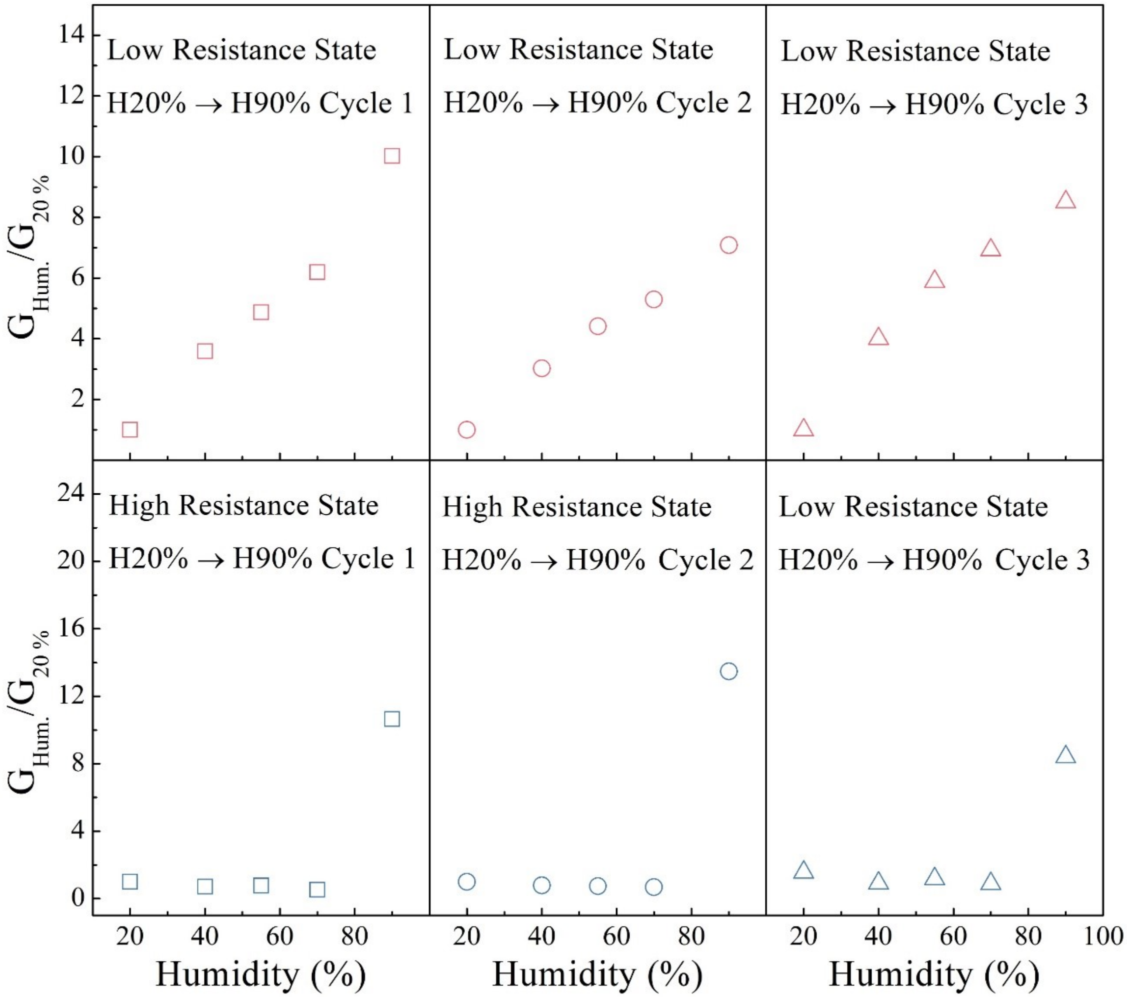

Fig. S8. Reversibility test of conductance changes (LRS and HRS) under different humidity levels.

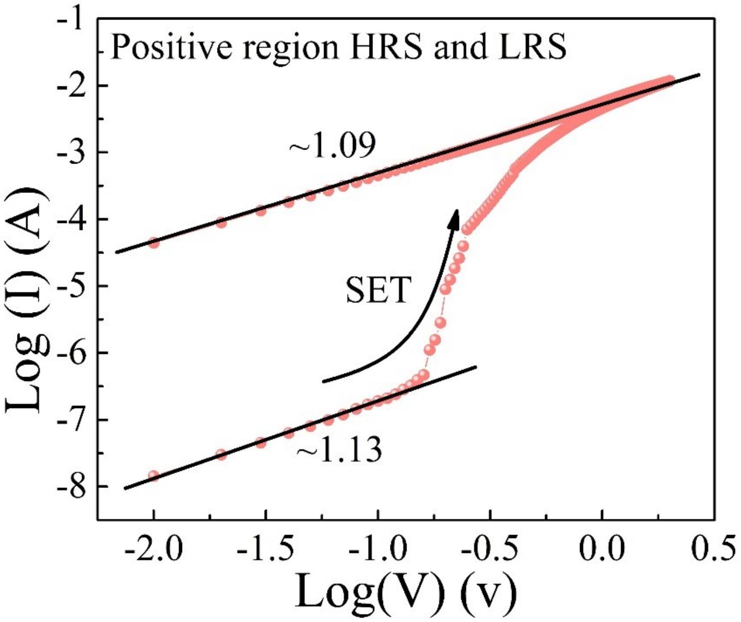

Fig. S9. The direct current (DC) switching cycle test of the device in the log (I)–log(V) scale (positive region).

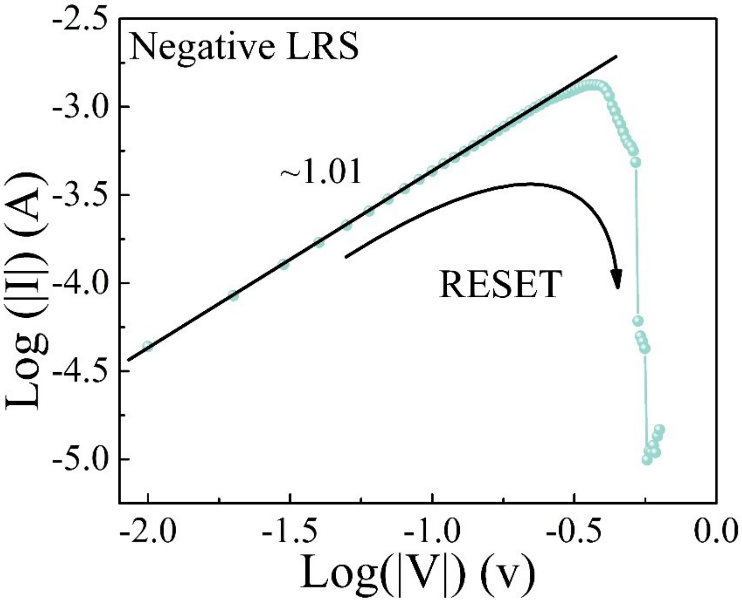

Fig. S10. The direct current (DC) switching cycle test of the device in the log (I)–log(V) scale (negative region).

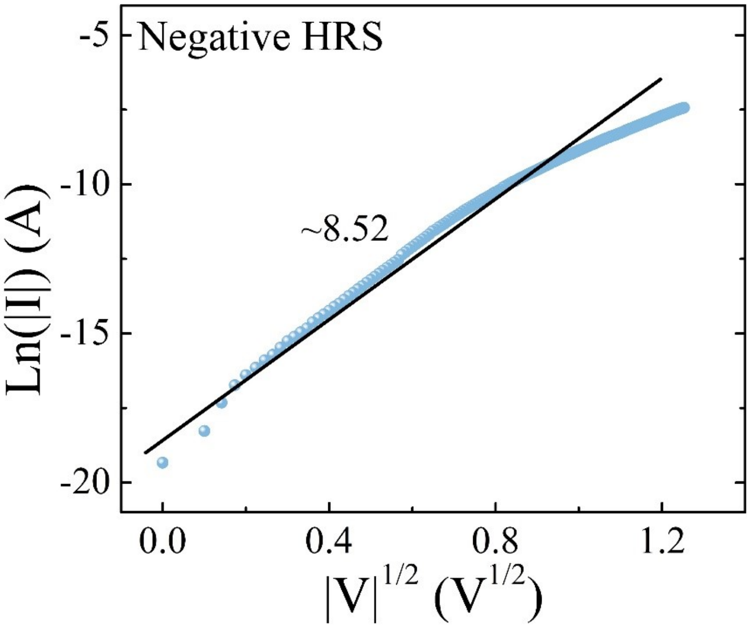

Fig. S11. The direct current (DC) switching cycle test of the device in the $V^{1/2}$– Ln(I) scale (negative region).

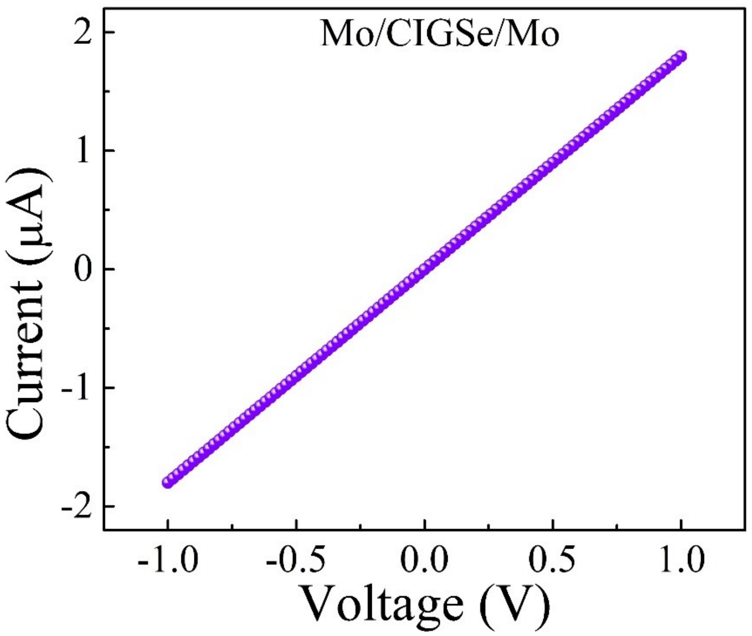

Fig. S12. The direct current (DC) switching cycle test of the Mo/CIGSe/Mo. The sweep voltage was 0 → 1 V → -1 V → 0 V.

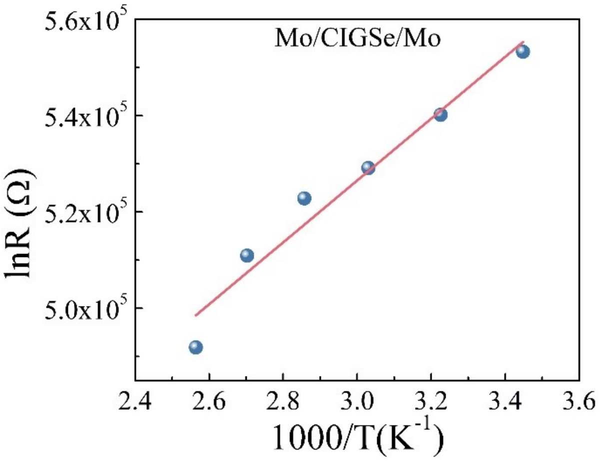

Fig. S13. Resistance changes of Mo/CIGSe/Mo under different temperatures.

When the device was at the HRS, the conductive feature was determined by the semiconductive CIGSe layer.[1] The conductance of the device increased with the increase of temperature. Because a higher temperature induces a higher density of carriers that determined the overall conductivity ability.[2] To further confirm the semiconductive temperature-depended conductance (or resistance) changes. The device of Mo/CIGSe/Mo was also tested under different temperatures as shown in Fig. S13. Inert Mo was used as the top electrode. The Ohmic contact forms at the interface of Mo/CIGSe, which eliminates the influence of the Schottky barrier.[3] The influence of temperature on the semiconductive CIGSe was investigated. The resistance decreased with the increase of temperature (conductance increases with the increase of temperature), which is consistence with the HRS of the memristive device in this paper. Meanwhile, the conductivity of semiconductors is determined by the density of electrons that are excited from the valence band to the conduction band. The required energy to excite the electrons from the valence band to the conduction band is described by Equation S1:[4]

$$\Delta E = E_c - E_v \qquad \text{S1}$$

where E_c is the conduction band edge, and E_v is the valence band edge. The conductivity σ is proportional to the number of carriers (or electrons) in the conduction band. The resistivity ρ is the inverse of the conductivity σ, one can find the following Equation S2:

$$\rho = \frac{1}{\sigma} = B^{'} e^{\frac{E_c - E_v}{kT}} \qquad \text{S2}$$

where B' is an empirical constant. k is the Boltzmann constant. T is the temperature. The resistance can be described by Equation S3:

$$R = \rho \frac{L}{S} \qquad \text{S3}$$

where R is the resistance value. L is the length of measured materials (thickness of the active layer in this work). S is the cross-section area of measured materials (the device area in this work). Combining the Equation S2 and S3, one can find the following Equation S4:

$$R = Be^{\frac{E_c - E_d}{kT}} \qquad \text{S4}$$

where B is a constant. Equation S4 can be transformed into the following form.

$$\ln{(R)} = \ln{(B)} + \frac{E_c - E_d}{kT} \qquad \text{S5}$$

Therefore, in a semiconductive system, the ln(R) and 1/T have a linear relation. The experimental results are shown in Fig. S13, a linear relation can be observed. It further confirmed the semiconductive features of the CIGSe layer.[5]

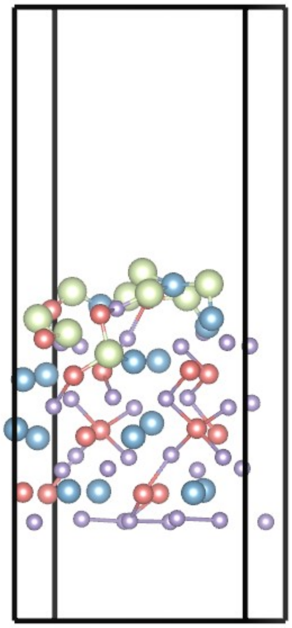

Fig. S14. The theoretical model of the CIGSe-O (CIGSe crystal surface bonding -O groups). The corresponding element and representative ball colors are consistent with the demonstration in Figure 3.

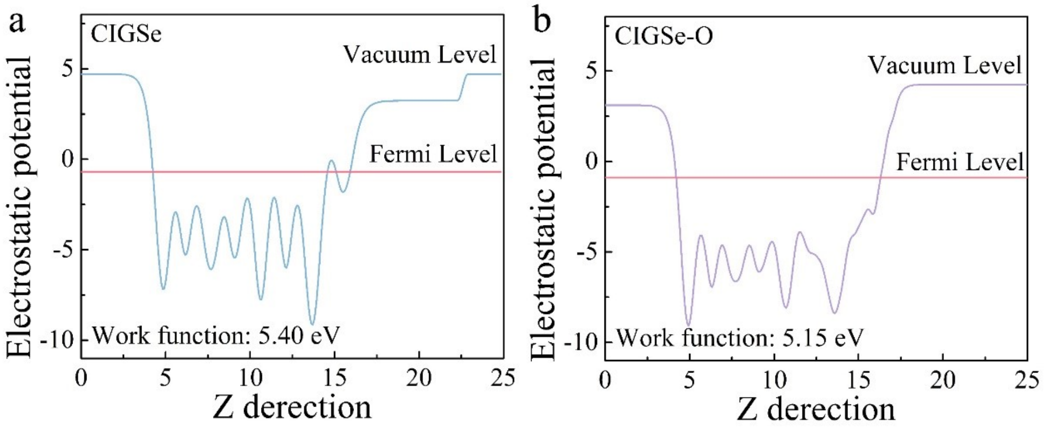

Fig. S15. (a) The electrostatic potential distribution along the Z direction of CIGSe. (b) The electrostatic potential distribution along the Z direction of CIGSe bonded O-group.

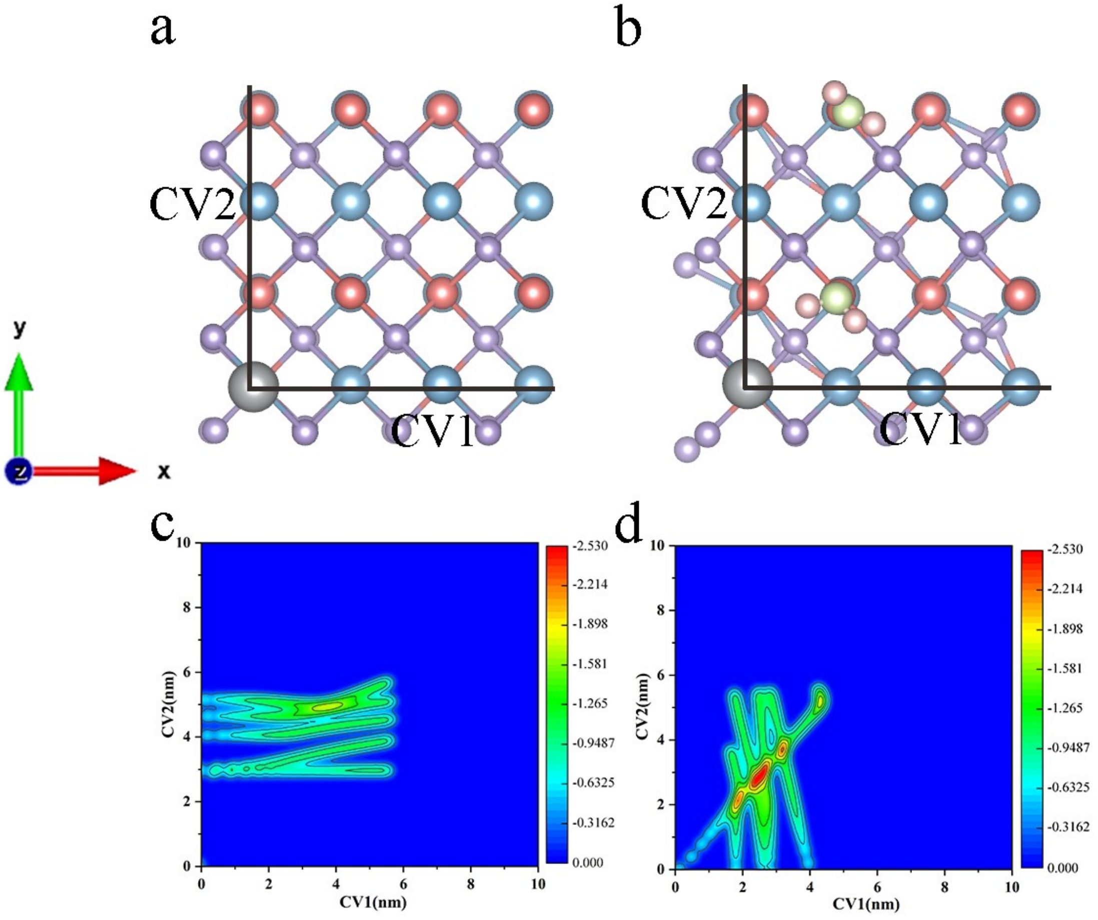

Fig. S16. (a) Theoretical model of the CIGSe without H_2O molecules. (b) Theoretical model of the CIGSe with H_2O molecules on the surface. (c) Free energy mapping of Ag atoms on the crystalline surface. (d) Free energy mapping of Ag atoms on the crystalline surface with bonded H_2O molecules. The corresponding element and representative ball colors are consistent with the demonstration in Figure 4.

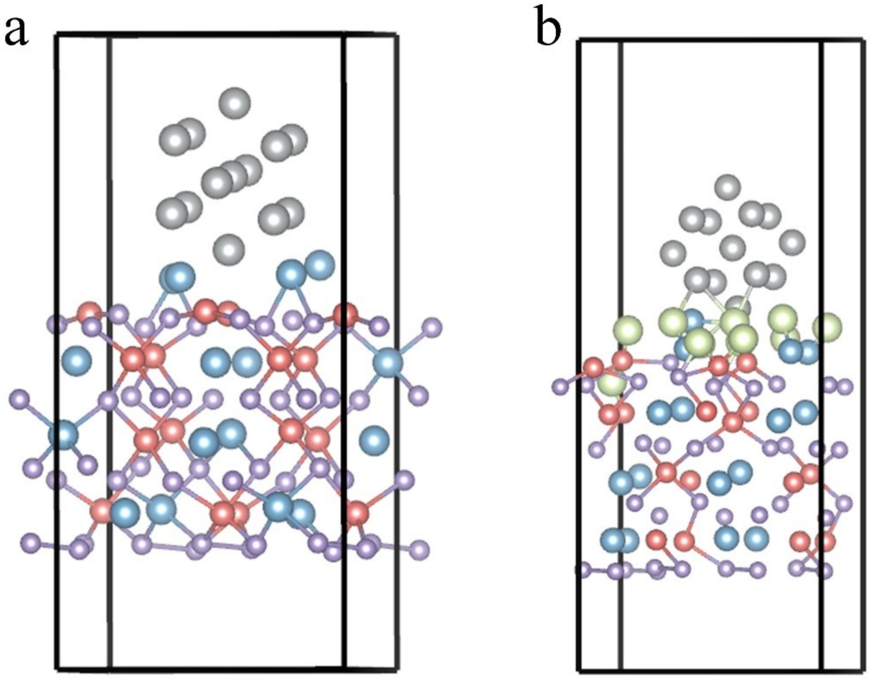

Fig. S17. The theoretical model of (a) CIGSe-Ag systems and (b) CIGSe-O-Ag systems. The corresponding element and representative ball colors are consistent with the demonstration in Fig. 4.

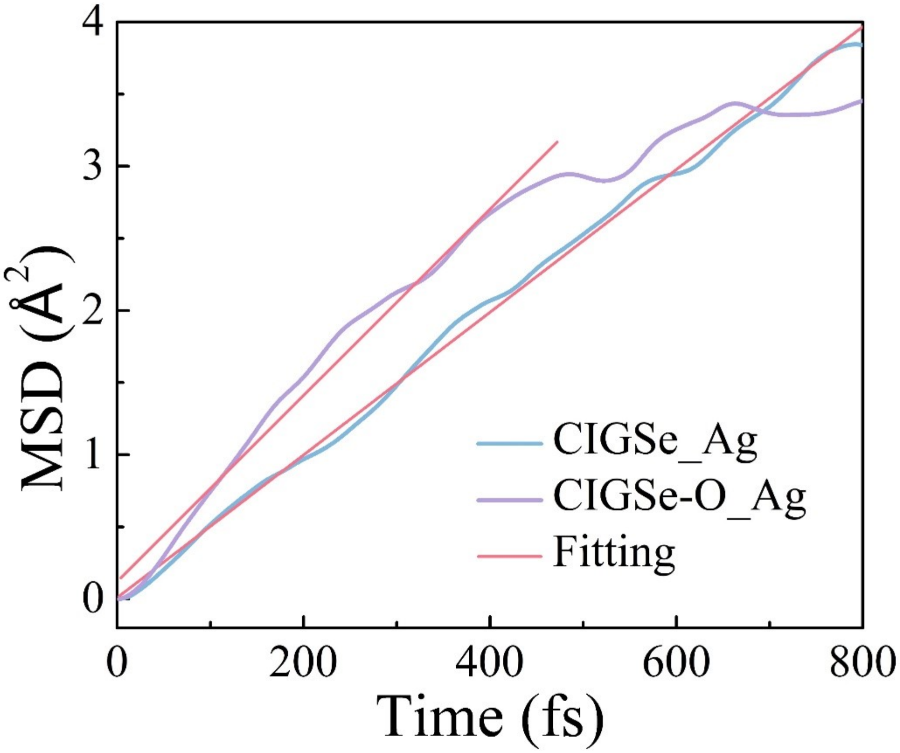

Fig. S18. Mean square displacement (MSD) from Ab Initio molecular dynamics calculations (AIMD) analysis for CIGSe_Ag and CIGSe-O_Ag systems.

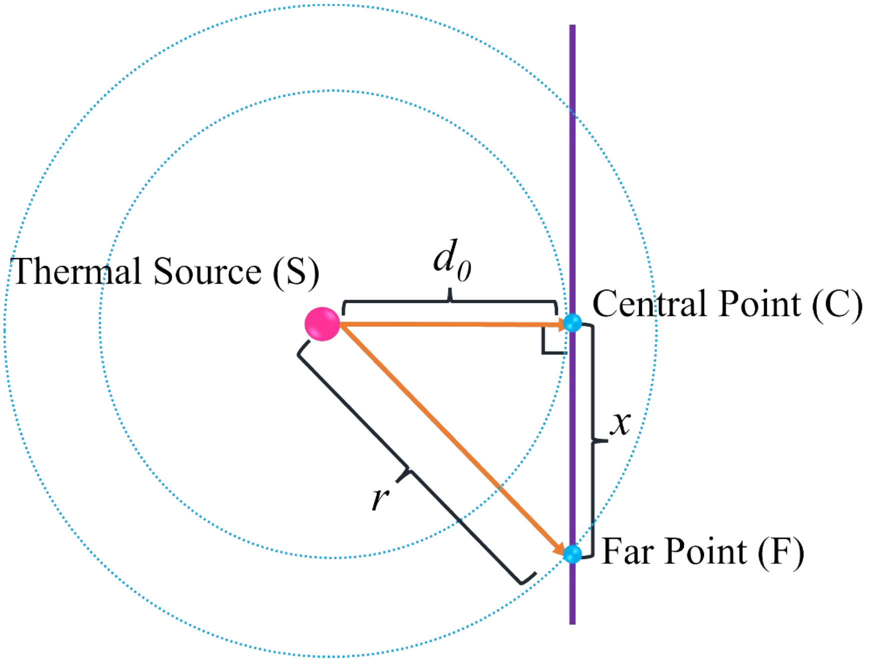

Fig. S19. Schematic diagram for the calculation of thermal transmission distribution in one direction. The thermal source is assumed as a point. A constant amount of energy is spread out in an expanding sphere as it is transmitted away from the source. The thermal intensity at a certain point is described by Equation S6.

$$S_F = \frac{P}{4\pi r^2} \qquad \text{S6}$$

where S_F is the thermal radiation intensity at a specific point F. P is the total energy released per second. r is the distance between the light source and the specific point (the length of SF in Fig. S19, ESI†). The thermal radiation intensity at the point F is described by Equation S7:

$$S_F = \frac{d_0^2}{x^2 + {d_0}^2} S_C \qquad \text{S7}$$

where S_C is the thermal radiation intensity at the central point C in Fig. S19 (ESI†). The normalized thermal radiation intensity is shown in Fig. S20 (ESI†). The thermal energy density decreased quickly as the points get away from the central point. Mathematical manipulation can extend the thermal energy distribution from a one-dimensional space to a two-dimensional plane, which describes the thermal distribution more accurately and visually. The thermal energy distribution on the two-dimensional surface is shown in Fig. 4b_1.

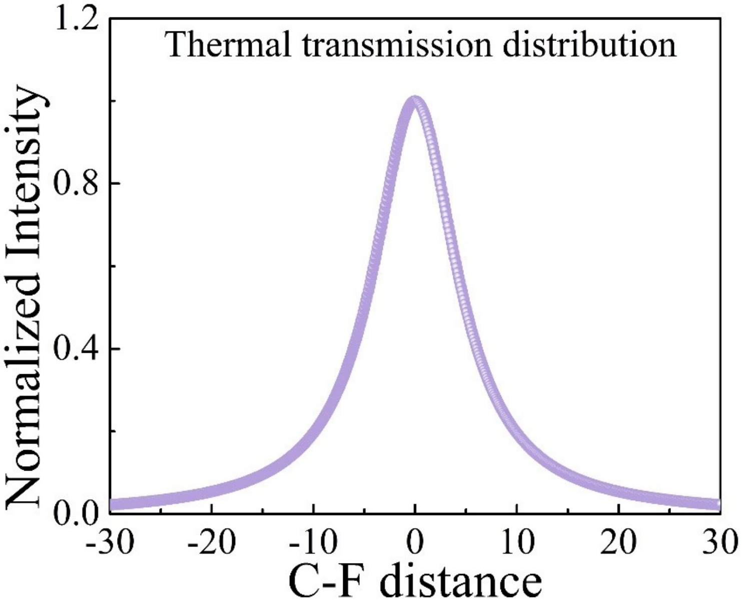

Fig. S20. Theoretical simulation of the thermal transmission distribution in one direction. The X and Y coordinates are C-F distance and normalized intensity of thermal energy respectively. The d_0 (S-C distance) is presumed to be 5.

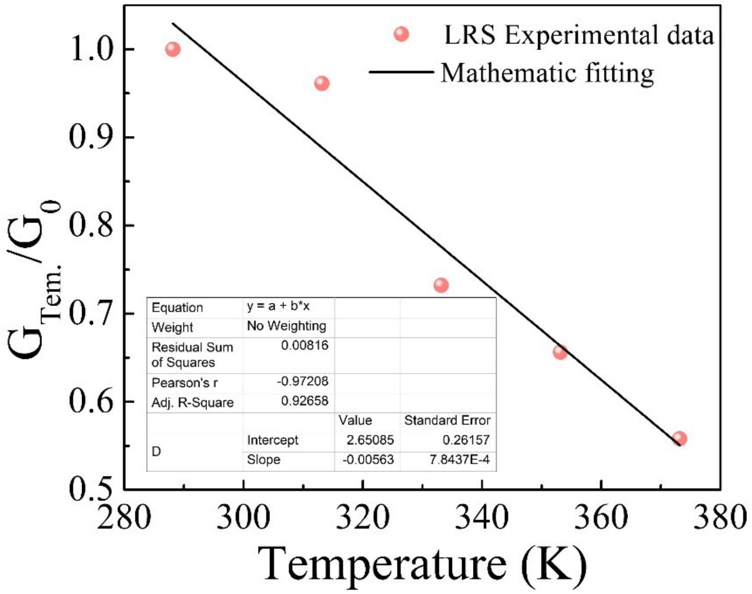

Equation	y = a + b*x		
Weight	No Weighting		
Residual Sum of Squares	0.00816		
Pearson's r	-0.97208		
Adj. R-Square	0.92658		
D		Value	Standard Error
	Intercept	2.65085	0.26157
	Slope	-0.00563	7.8437E-4

Fig. S21. The change of $G_{Tem.}/G_0$ under different temperatures at the LRS model. $G_{Tem.}$ represents the conductance at a specific temperature. G_0 is the conductance at room temperature (288K). The solid line is the linear mathematic fitting to the experimental data. The insert table is the fitting parameters.

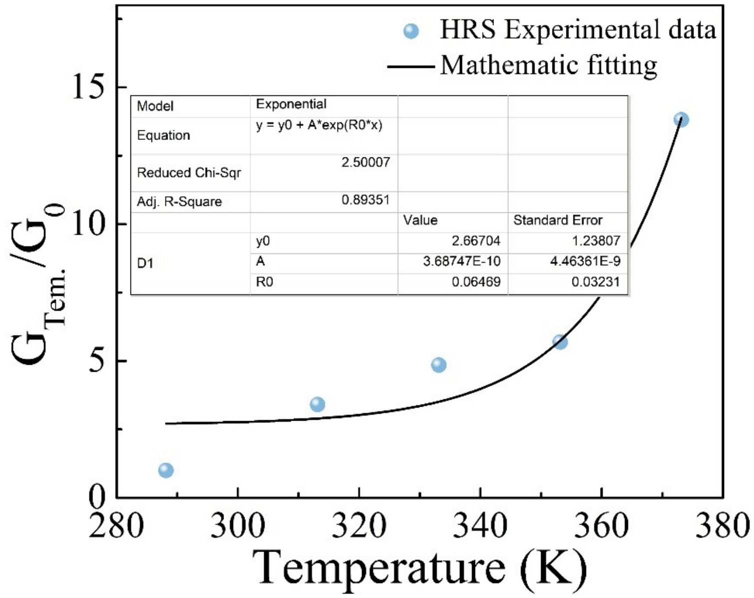

Model	Exponential		
Equation	y = y0 + A*exp(R0*x)		
Reduced Chi-Sqr	2.50007		
Adj. R-Square	0.89351		
		Value	Standard Error
D1	y0	2.66704	1.23807
	A	3.68747E-10	4.46361E-9
	R0	0.06469	0.03231

Fig. S22. The change of $G_{Tem.}/G_0$ under different temperatures at the HRS model. $G_{Tem.}$ represents the conductance at a specific temperature. G_0 is the conductance at room temperature (288K). The solid line is the exponential mathematic fitting to the experimental data. The insert table is the fitting parameters.

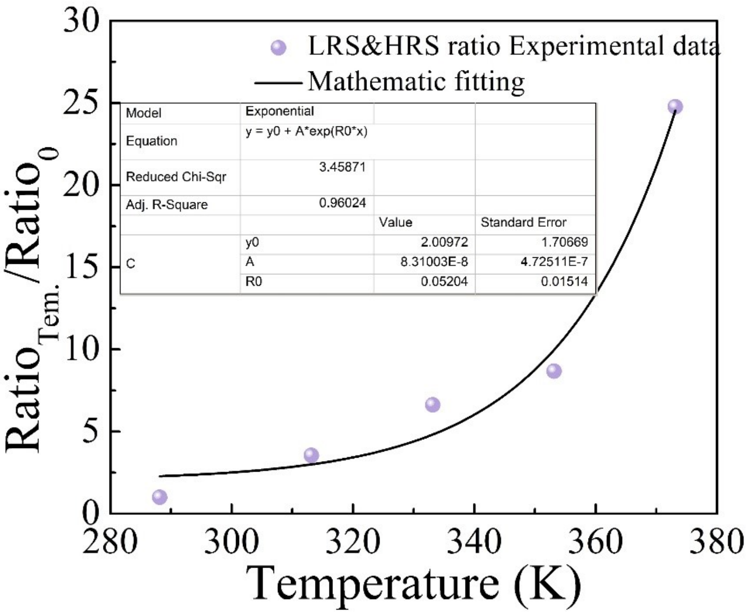

Model	Exponential		
Equation	y = y0 + A*exp(R0*x)		
Reduced Chi-Sqr	3.45871		
Adj. R-Square	0.96024		
		Value	Standard Error
C	y0	2.00972	1.70669
	A	8.31003E-8	4.72511E-7
	R0	0.05204	0.01514

Fig. S23. The change of $\mathrm{Ratio}_{\mathrm{Tem.}}/\mathrm{Ratio}_0$ under different temperatures at the HRS&LRS model. $\mathrm{Ratio}_{\mathrm{Tem.}}$ represents the ratio of LRS/HRS at a specific temperature. Ratio_0 is the ratio of LRS/HRS at room temperature (288K). The solid line is the exponential mathematic fitting to the experimental data. The insert table is the fitting parameters.

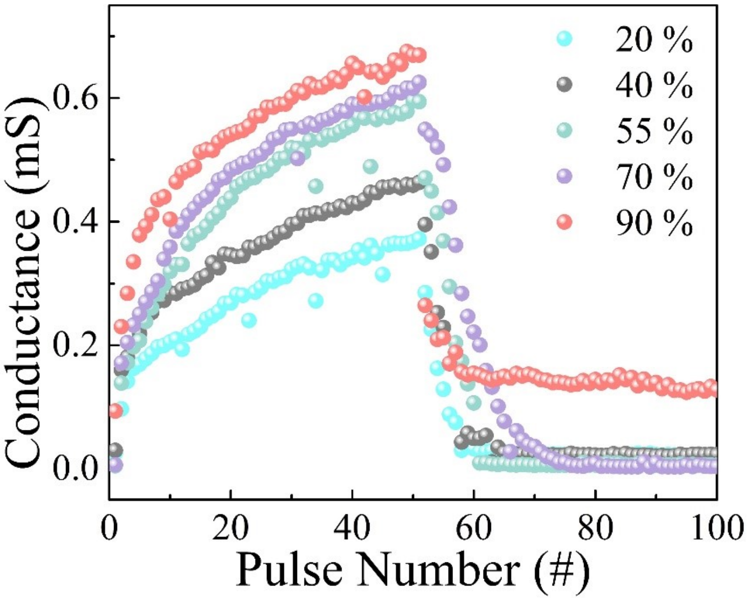

Fig. S24. Electronic potentiation/depression characterizations under different humidity levels.

Reference

1 N. Mufti, T. Amrillah, A. Taufiq, Sunaryono, Aripriharta, M. Diantoro, Zulhadjri and H. Nur, *Sol. Energy*, 2020, **207**, 1146–1157.
2 K. Seeger, *Semiconductor Physics*, Springer Science & Business Media, 2013.
3 K. Sardashti, R. Haight, R. Anderson, M. Contreras, B. Fruhberger and A. C. Kummel, *ACS Appl. Mater. Interfaces*, 2016, **8**, 14994–14999.
4 R. A. Butera and D. H. Waldeck, *J. Chem. Educ.*, 1997, **74**, 1090.
5 Y. Wang, R. Wenisch, R. Schlatmann and I. Lauermann, *Adv. Energy Mater.*, 2018, **8**, 1801692.